EarthArXiv Cover Sheet

Title

Reconstructing Spatial Denudation Patterns in a Reverse-Engineered Fluvial Catchment

Authors

Dnyanesh Borse[1] (ORCID: 0000-0002-5140-2427)
Arvind Singh[1] (ORCID: 0000-0003-2172-6321)
Gary Parker[2,3] (ORCID: 0000-0001-5973-5296)

[1]Department of Civil, Environmental, and Construction Engineering, University of Central Florida, Orlando, FL, USA.
[2]Dept. of Earth Science and Environmental Change, University of Illinois Urbana-Champaign, Urbana, IL 61801.
[3]Dept. of Civil and Environmental Engineering, University of Illinois Urbana-Champaign, Urbana, IL 61801.

Main Manuscript for

Reconstructing Spatial Denudation Patterns in a Reverse-Engineered Fluvial Catchment

Dnyanesh Borse[1], Arvind Singh[1], and Gary Parker[2,3]

[1]Department of Civil, Environmental, and Construction Engineering, University of Central Florida, Orlando, FL, USA.

[2]Dept. of Earth Science and Environmental Change, University of Illinois Urbana-Champaign, Urbana, IL 61801.

[3]Dept. of Civil and Environmental Engineering, University of Illinois Urbana-Champaign, Urbana, IL 61801.

Corresponding author: Arvind Singh (Arvind.Singh@ucf.edu)

Key Points:

- Hydraulic-geometry-based sediment flux predicts spatially resolved denudation in landscapes.
- Denudation systematically decreases downstream, reflecting drainage-area scaling of sediment transport.
- Network structure sets spatial patterns; climate, sediment and regolith properties regulate erosion magnitude.

Author Contributions: D.B. implemented the computational framework, performed the analyses, interpreted the results, and wrote the manuscript. A.S. contributed to the study design, interpretation of the results, and manuscript preparation. G.P. conceived the study, provided overall conceptual guidance and integration, and contributed to writing the manuscript.

Competing Interest Statement: The authors declare no competing interests.

Keywords: Denudation, Hydraulic geometry, Sediment transport, Drainage networks, Reverse Engineered Fluvial Landscape, Landscape evolution

Abstract

Quantifying the spatial heterogeneity of denudation rates is a challenge in geomorphology, particularly in tectonically subdued montane landscapes. We develop a sediment flux-based framework to estimate spatial denudation using a generic reverse-engineered fluvial catchment. The model combines physically based hydraulic geometry with a sediment transport relation to compute gravel flux throughout the channel network using bankfull discharge and grain size. Denudation rates are related to gravel flux and the associated contributing hillslope area through the assumption that denuded material contains a constant fraction of gravel depending on lithology and weathering. We found that the drainage network controls the spatial pattern, whereas climate and sediment/regolith properties control denudation magnitude, which decreases toward the catchment outlet. Sensitivity analyses evaluate the effects of basin scale, grain size, precipitation intensity, and gravel fraction on denudation variability. Our framework provides a computationally efficient approach for estimating spatial denudation in landscapes with sparse geochronological data.

Plain Language Summary

Landscapes gradually wear down as rivers and streams transport sediment away from hillslopes, a process known as denudation. Measuring how rapidly this occurs across different parts of a landscape remains challenging because direct measurements are often sparse and limited to a few locations. In this study, we present a new method to estimate denudation rates using the amount of sediment transported by river networks. Starting from a computer-generated river basin satisfying known scaling relations for a class of fluvial catchments, we use well-established hydraulic relationships to calculate how much gravel and finer sediment rivers can move at different locations within the network. We then convert these sediment transport rates into estimates of how quickly the surrounding landscape is being lowered. Our results specifically justify the observation that denudation rates are generally higher in upper regions of the river network and decrease downstream. We also test how sensitive these estimates are to factors such as basin size, sediment grain size, rainfall intensity, and the proportion of gravel in the transported sediment. This approach offers a computationally efficient method for estimating spatial denudation rates in a class of data-sparse landscapes.

1 Introduction

Denudation refers to the long-term lowering of Earth's surface through the combined effects of weathering, erosion, and sediment transport (Anderson & Anderson, 2010; Summerfield, 2014). Quantifying denudation rates is central to understanding landscape evolution because it links surface processes to topography, sediment budgets, and hydrologic forcing (Anderson et al., 2002; Dietrich et al., 2013; Tucker & Hancock, 2010; Whipple, 2004). Spatial heterogeneity in denudation controls relief development, drainage organization, and long-term geomorphic stability (Montgomery & Brandon, 2002).

Traditional approaches to estimating denudation rates often rely on cosmogenic radio nuclides such as ^{10}Be or thermochronological techniques (Brown et al., 1995; Lal, 1991; Portenga & Bierman, 2011; Reiners & Brandon, 2007). While powerful, these methods require extensive field sampling, laboratory processing, and assumptions about production rates, exposure history, and sediment mixing (Bierman & Nichols, 2004; Granger et al., 1996). As a result, spatial coverage is typically sparse, and extrapolation to basin-wide denudation patterns remains challenging (von Blanckenburg, 2005; Portenga & Bierman, 2011). In addition, these methods in and of themselves are silent in regard to the physical processes that cause denudation (Dietrich et al., 2013).

In the case of tectonically subdued montane landscapes, relief is modest, uplift rates are low, and sediment transport is often transport-limited rather than detachment-limited (Tejedor et al., 2017; Tucker & Hancock, 2010; Whipple & Tucker, 2002; Willgoose et al., 1991). Many widely used landscape evolution formulations, including the stream power incision model (e.g., Howard, 1994; Whipple, 2004; Whipple & Tucker, 1999) are most appropriate for bedrock-dominated, incision-controlled systems. Their direct application to low-relief montane catchments drained by alluvial gravel-bed rivers can therefore misrepresent the dominant mechanics governing sediment flux and surface lowering (Whipple & Tucker, 2002).

In transport-limited systems, denudation is related primarily to sediment transport capacity and channel hydraulics rather than to bedrock incision thresholds (Whipple & Tucker, 2002). Hydraulic geometry relationships describe systematic downstream variations in channel width, depth, slope, and discharge, providing a physically based link between water flux and sediment transport (Leopold & Maddock, 1953). Parker et al. (2007) developed a dimensionally homogeneous framework that relates bankfull discharge to channel width, depth, slope, and gravel transport rate through principles of mass and momentum conservation, flow resistance, and sediment transport mechanics. Because these relations are scalable and physically grounded, they provide a natural basis for estimating sediment flux throughout drainage networks.

Under long-term quasi-equilibrium conditions, sediment flux exported through a channel network reflects the rate at which material is removed from the landscape (Willett & Brandon, 2002). Consequently, spatial variations in channel geometry and sediment transport capacity can be related to spatial variations in denudation (Attal et al., 2015). This perspective is particularly attractive in tectonically subdued landscapes, where channel hydraulics and sediment mobility exert a stronger influence on landscape lowering than bedrock incision processes. Existing sediment-flux-based frameworks (Milliman & Syvitski, 1992; Syvitski & Milliman, 2007) infer denudation from basin-outlet sediment yields, providing only basin-averaged rates rather than spatial detail. Here we develop a new sediment-flux-based framework that combines hydraulic geometry and sediment transport theory to estimate spatial denudation rates across a generic transport-limited drainage basin with alluvial gravel bed channels. We then examine how denudation patterns vary with basin area, grain size, discharge, and sediment composition. This framework provides a computationally efficient and physically grounded approach for estimating spatial heterogeneity in denudation across tectonically quiescent, transport-limited landscapes, where direct field-based constraints are often sparse.

2 Materials and Methods

In this study, we develop a sediment-flux-based framework to estimate spatial denudation patterns in transport-limited fluvial landscapes. We demonstrate the framework using the Reverse Engineered Fluvial Landscape (REFL) methodology developed by Zhang et al. (2026a), which incorporates physically based hydraulic geometry relations (Parker et al., 2007) to calculate channel-scale gravel transport rates. These transport rates are then converted into spatially distributed denudation rates.

The REFL framework utilizes a two-parameter probabilistic model for generating scale-free two-dimensional drainage networks (see Borse & Biswal, 2023). It then generates a three-dimensioned landscape using physically based dimensionally homogeneous hydraulic geometry relations for alluvial gravel-bed rivers (Parker et al., 2007) and a simplified hillslope representation characterized by an effective hillslope length L_h and hillslope slope S_h calibrated using the Britain II dataset (Hey & Thorne, 1986; Zhang et al., 2026a) (details in Text S1 of Supporting Information). An example of a scale-free drainage network generated by the REFL approach is shown in Fig. 1a. The dimension-free networks are scaled to physical lengths in kilometers using a multiplicative scaling parameter λ. Hydraulic geometry relations are then used to calculate channel slope S, bankfull width B_{bf}, bankfull depth H_{bf}, and bankfull gravel transport rate $Q_{b,\mathrm{bf}}$ from bankfull discharge Q_{bf} and characteristic surface grain size D (Parker et al., 2007). Channel elevations are reconstructed from the calculated slopes, and the surrounding topography is generated using effective hillslope parameters providing a 3D landscape (Fig. 1b and 1c).

We employ an empirical rational method for bankfull discharge $\left(Q_{bf}\right)$ based on catchment area (A), where Q_{bf} is expressed as a linear function of drainage area as $Q_{bf} = aA$. The coefficient a represents a regional scaling factor, A is in km^2 and Q_{bf} is in m^3/s. To ensure dimensional homogeneity and allow climatic variation, this relation is expanded so as to include flood intensity and duration intermittency within the framework:

$$Q_{bf} = aA \qquad [1a]$$

$$Q_{bf} = a_{flood} i_{flood} I_{flood} A, \quad a = a_{flood} i_{flood} I_{flood} \qquad [1b]$$

where, i_{flood} represents the effective precipitation rate during near-bankfull events, I_{flood} is the fraction of time the river remains near bankfull flow, and a_{flood} is a dimensionless coefficient. Details about model parameters are in Text S2 of SI.

To quantify sediment flux, we utilize the hydraulic geometry framework for gravel-bed rivers of Parker et al. (2007). This framework defines dimensionless discharge $\hat{Q}$ and dimensionless gravel transport rate $\hat{Q}_{b,bf}$ as follows and then provides a relationship between $\hat{Q}_b$ and $\hat{Q}$.

$$\hat{Q} = \frac{Q_{bf}}{\sqrt{gD}D^2}, \; \hat{Q}_b = \frac{Q_{b,bf}}{\sqrt{gD}D^2} \qquad [2a]$$

$$\hat{Q}_b = \alpha_y \hat{Q}^{n_y} \quad [2b]$$

where the coefficient $\alpha_y = 0.0033$ and the exponent $n_y = 0.551$ apply to alluvial gravel-bed rivers (see, Parker et al., 2007, for details). Wilkerson & Parker (2010) obtained a similar value of n_y of 0.602 for alluvial sand-bed rivers. The relation itself is based on a back-calculation from a) observed bankfull hydraulic geometry relations for alluvial gravel-bed rivers developed from and verified with data from the Rocky Mountains, USA, the Appalachian Mountains, USA and the United Kingdom (including the Britain II dataset mentioned above) and b) a framework that captures the physical basis for these relations.

To translate localized river transport into a landscape-wide signal, we link the denudation of competent gravel (D_{eg}) to the total hillslope denudation rate (D_{et}). Sediment is supplied to the rivers in a catchment from regolith eroded from adjacent hillslopes (e.g. Sklar, 2024). This material generally consists of a wide range of sizes and lithologies. Of relevance here is the fraction of this material retained as competent gravel on the streambed; the rest can be assumed to be transported through the channels as suspended load (Turowski et al., 2010) that is here treated as washload in the context of bed sediment.

We thus assume that sediment delivered from hillslope to channel in the form of competent gravel is a dimensionless fraction (ω) of the total material sediment delivered:

$$D_{eg} = \omega D_{et} \quad [3]$$

Furthermore, we relate the mean annual gravel transport rate (Q_b) to the bankfull gravel transport rate ($Q_{b,bf}$) using the intermittency coefficient (I_{flood}) (Paola et al., 1992)

$$Q_b = I_{flood} Q_{b,bf} \quad [4]$$

The denudation rate of the subarea A draining into a given channel location can be related to the mean annual gravel transport rate at that location as follows:

$$Q_b = I_{flood} Q_{b,bf} = \int \omega D_{et} dA \quad [5a]$$

or thus

$$I_{flood} \frac{dQ_{b,bf}}{dx} = \omega D_{et} A \quad [5b]$$

These relations are general and not limited to the specific class of catchments considered here. Equations (1b), (2b), (4) and (5b) yield:

$$Q_{b,bf} = a_y A^{n_y} \quad where \quad a_y = \alpha_y \gamma^{(1-n_y)} a^{n_y} \text{ and } \gamma = \sqrt{gD} \times D^2 \quad [6a]$$

for the class of catchments considered here. We equate the mean annual gravel transport rate at any point along a river in the network to the integral of the denudation rate over the area that drains into that point. From Equations (3). (4), (5b) and (6a)

$$I_f \frac{dQ_{b,bf}}{dA} = I_f a_y n_y A^{n_y - 1} = \omega D_{et} \quad [6b]$$

or thus

$$D_{et} = \frac{I_f a_y n_y}{\omega} A^{-m_y} \,,\;\; m_y = 1 - n_y > 0 \; and \;\; a_y = \; \alpha_y \gamma^{(1-n_y)} a^{n_y} \quad [6c]$$

Equation (6c) is dimensionally homogeneous in light of Equations (1b) and (6a). The annual denudation rate predicted from Equation (6c) should be treated as a value corresponding to long-term geomorphological evolution rather than for any specific year. In our implementation n_y takes the above-quoted value 0.577, in which case m_y = 0.423. Equation (6c) thus specifically corresponds to a denudation rate that increases with decreasing drainage area. The area draining into a given channel pixel is expressed (see Figure 1d) as the sum of the areas of all hillslope pixels into that channel pixel. All these hillslope pixels draining to a channel pixel are assumed to have the same denudation rate. The process of delivery of denuded sediment to the channel is illustrated in Figure 1e.

The value of ω, i.e. the fraction of denuded sediment that is retained in the channel as competent gravel, is poorly constrained. It is presumably dependent upon hillslope bedrock lithology, the processes by which regolith is generated and regolith material is delivered to the channel. Turowski et al. (2010) provide some guidance in this regard. In their Table 3, they estimate representative values of the fraction of total load in gravel-bed streams that is transported as bedload rather than suspended load as ranging from 0.26 for relatively low suspended load concentrations to 0.088 for relatively high suspended load concentrations. The drainage networks in question do not necessarily correspond to those considered here but can be used for the purpose of making estimates. While bedload does not necessarily correspond to gravel, Parker et al. (2024) have argued that sediment coarser than 5 mm is rarely transported in suspension in significant quantities in alluvial rivers. With this in mind, values of ω ranging from 0.1 to 0.3 are considered here.

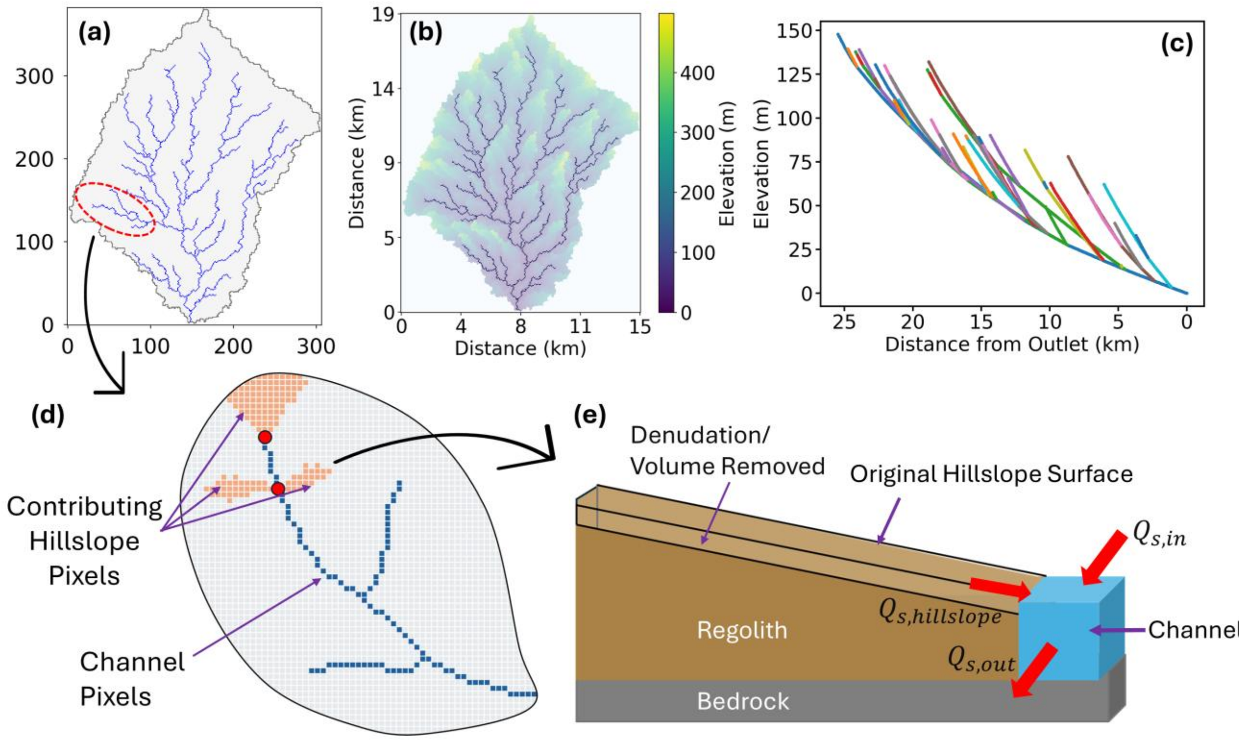

Figure 1. Panel (a) shows a 2D scale free network obtained using probabilistic algorithm and Panel (b) illustrates a 3D reverse engineered fluvial landscape. Panel (c) shows the long profiles for the main stem and all tributaries. Panels (d) and (e) illustrate the denudation calculation framework based on gravel transport rates. Gravel transport rates are first calculated for each channel pixel. The corresponding denudation rates are then estimated for hillslope pixels draining to each channel pixel. **(d)** Example showing the hillslope pixels contributing to two sample channel pixels. **(e)** Channel cross-section illustrates how sediment supplied from adjacent hillslopes contributes to the channel gravel load.

3 Results

The scale-free yet realistic 2D channel network generated using probabilistic algorithm within an arbitrarily shaped basin is shown in Fig. 1a and the corresponding 3D reverse engineered landscape is shown in Fig 1b (see Borse & Biswal, 2023; Zhang et al., 2026a). This landscape characterizes a generic low-slope montane catchment with subdued tectonics whose drainage area is 152 km^2, main channel length is 25.5 km and relief is 499 m. The parameters used to construct this landscape are: D=59 mm, L_h=500 m (corresponding to a drainage density of 0.001 m^{-1}) and S_h=0.1 In addition, i_{flood}=2.59 mm/hr and I_{flood} = 0.01, yielding the value a = 0.52. Figure 1c shows the channel profile for the main stem along with all tributaries for this basin.

Fig. 2a shows the modeled mean annual gravel transport rate (annual gravel yield) at every point in the channel network. As can be seen from Fig. 2b, the modeled gravel transport rate using the proposed framework (Equation 5b) increases monotonically downstream toward the outlet of the catchment. The outlet gravel yield of 2133 tons/year represents the contribution from the entire catchment upstream. The spatial pattern of sediment yield demonstrates the hierarchical aggregation of sediment flux within the basin.

The information derived from the reconstructed 3D landscape (Fig. 1b), together with Equation (6c), yields key result of the present analysis: the spatial distribution of denudation rate across the entire catchment, shown in Figure 2b. We refer to this as the Base Case. Note that we have used $\omega = 0.2$ to obtain the denudation rates shown in Figure 2b and subsequent figures unless mentioned otherwise. The denudation rate map (Fig. 2b) shows relatively elevated erosion in upstream and mid-basin regions, with spatial heterogeneity reflecting network structure and local drainage configuration. Denudation values range from minimum value of 0.015 mm/year at the outlet to 0.127 mm yr^{-1}, with higher rates generally associated with regions of lower drainage area and greater topographic relief. The spatial distribution indicates that erosion is not uniform across the basin but instead controlled by the organization of the drainage network. Particularly, headwater basins have higher denudation rates compared to hillslopes draining into side channels, as Equation (6) indicates that the local denudation rate decreases with increasing in drainage area.

We note that the REFL formulation for fluvial landscapes is not a landscape evolution model, and thus the present analysis cannot be used to make predictions many thousands or millions of years into the future. Since the present framework predicts the channel elevation-lowering rate to be equal to the denudation rate of the adjacent contributing hillslopes, we refer to the channel elevation-lowering rate as the main-stem denudation rate. Here we apply the denudation rates obtained from our model to estimate evolution of the landscape over time spans up to 1000 years. A linear extrapolation allows prediction of the longitudinal profile of denudation along the main stem (Fig. 2c). After the passage of a relatively short time (250 years), denudation is relatively low throughout the profile, with a maximum value of about 31.7 mm far upstream and a minimum value of 3.6 mm at the outlet. As time progresses (500–1000 years), denudation increases proportionally across the entire channel length. This pattern roughly aligns with the mature landscapes described in the cycle of erosion theory of Davis (1899). The main stem long profiles of Figure 2c show a step-like structure, reflecting discrete channel segments and network connectivity transitions.

The probabilistic nature of the 2D network generation model of Borse & Biswal (2023) allows different network realizations to be generated for the same parameter values while preserving the same statistical structure. Figures 2d and 2f show two sample 3D REFL landscape realizations (L1 and L2), referred to as Variant Cases 1 and 2, generated using the same input parameters as the Base Case. These cases show networks that are statistically the same as the Base Case, and in particular have the same drainage density, but differ in spatial organization. Figures 2e and 2g show their corresponding denudation patterns obtained using the same input parameters as the Base Case highlighting the spatial differences in the denudation patterns despite the similar range of overall denudation rate.

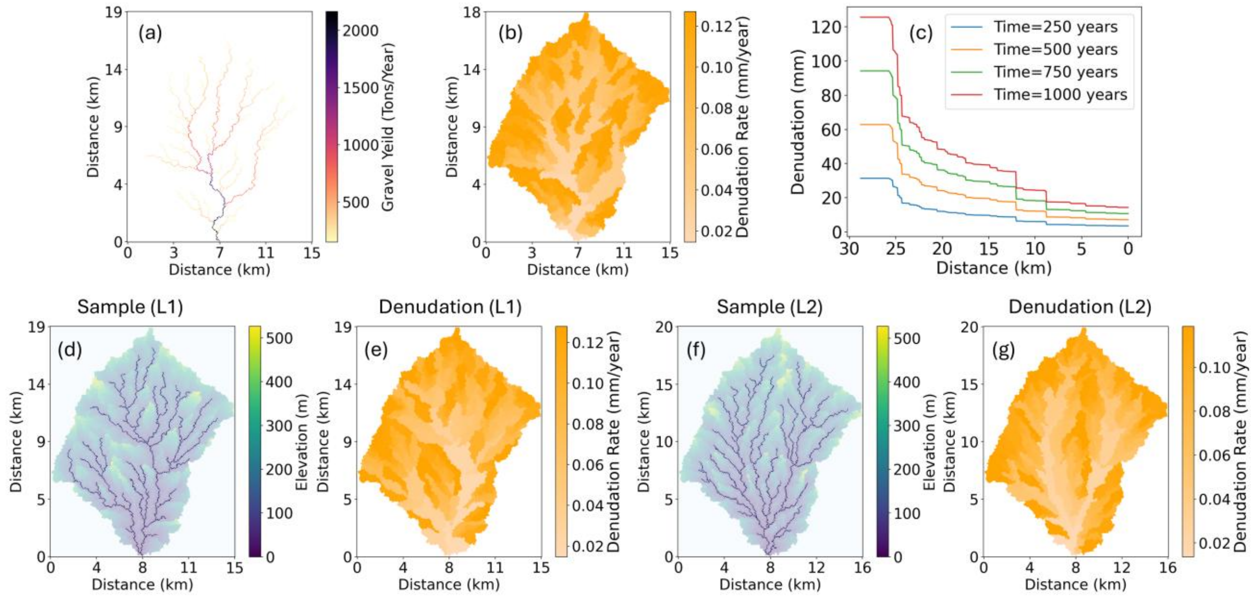

Figure 2. (a) In-channel gravel transport rate and (b) denudation rate for the Base Case; (c) main-stem denudation profile at different times; (d,e) Landscape (L1) and denudation rate for Variant Case 1; and (f,g) Landscape (L2) and denudation rate for Variant Case 2. Although the three cases differ in spatial detail, they exhibit similar ranges of denudation rates.

Figure 3 illustrates the sensitivity of longitudinal denudation profiles to variations in hydrologic forcing, sediment properties, and basin scale (see also Fig. S1-S4 and Table S1 in SI). In the Base Case, drainage area A = 152 km, the parameter $i_{flood} = 2.59$ mm/hr characterizing the hydrologic regime, characteristic channel bed surface grain size D = 59 mm and the fraction ω of denuded sediment that is retained as in-channel gravel = 0.2. As the parameter controlling effective precipitation rate (i_{flood}) increases from 1.94 to 3.88 (corresponding to bankfull discharge varying from 0.75 to 1.5 times the base case) while keeping other parameters constant, the denudation rates increase. This leads to a systematic upward shift in denudation rates along the entire channel system, with the strongest response observed in upstream reaches (Fig. 3a).

Similarly, increasing mean gravel size (D) enhances denudation magnitudes while preserving the overall downstream-decreasing structure of the profile (Fig. 3b), suggesting that grain size primarily modulates erosion intensity rather than spatial organization. In contrast, decreasing gravel fraction (ω) produces a pronounced increase in denudation, particularly in headwater regions (Fig. 3c), highlighting the role of sediment composition. Across basin sizes, larger drainage areas exhibit a broader range of and higher peak denudation values while maintaining a similar longitudinal decay pattern (Fig. 3d), indicating that spatial aggregation of flux amplifies erosion magnitude without altering its characteristic structure.

Figure 3e summarizes the variation in mean denudation rate as, i_{flood}, D, A and ω are individually varied from the Base Case. Mean denudation rates along the main stem are seen to range from 0.01 to 0.09 mm/yr across all cases tested in Figures 3a – 3d. Variation in gravel fraction ω produces the widest range of denudation rates. Variation in grain size D and drainage area A show comparable intermediate sensitivity, while variation in the hydrologic coefficient i_{flood} has the narrowest range, suggesting denudation is relatively robust to uncertainty in rainfall-runoff scaling. All parameters produce a consistent downstream decline in denudation rate (Fig. 3f), with the highest rates near the headwaters (0.1 – 0.25 mm/yr) decreasing toward the outlet (0.01–0.05 mm/yr), reflecting the decrease in unit stream power as drainage area increases and channel gradient reduces. Overall, the step-like longitudinal profile persists across all parameter variations, indicating that drainage network organization, particularly channel confluences, controls the spatial pattern of denudation, whereas model parameters primarily control its magnitude.

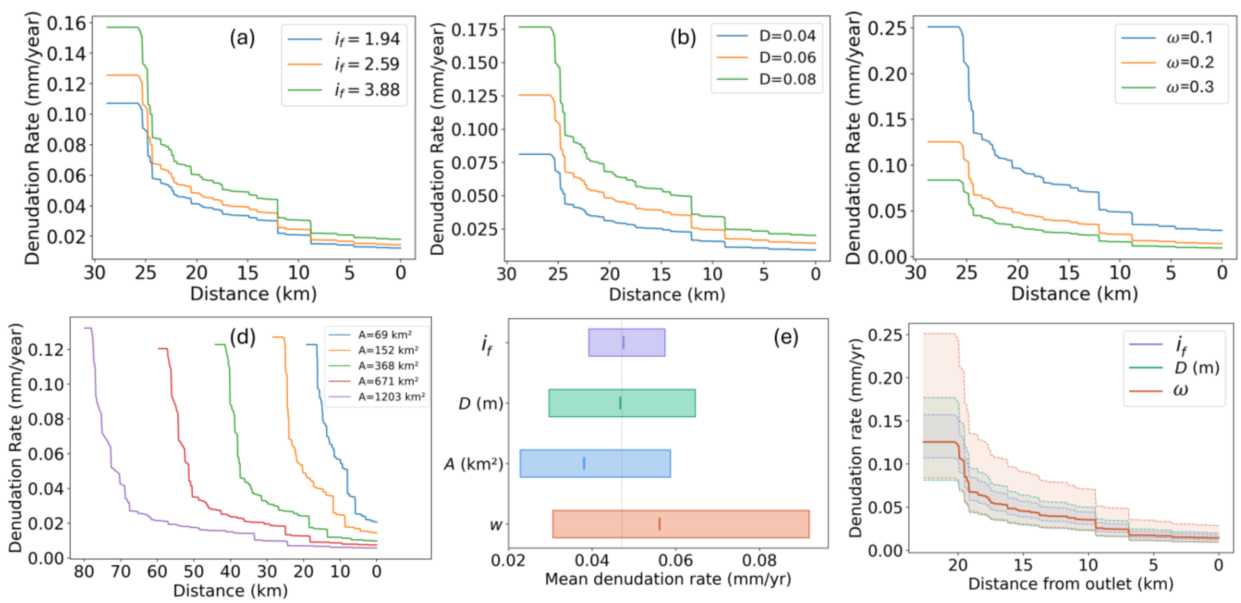

Figure 3. Sensitivity of modeled denudation rates along the main stem to key input parameters. (a) Denudation increases with increasing flood precipitation rate i_{flood} (shown as i_f) at constant flood intermittency $I_{flood} = 0.01$; (b) Denudation increases with mean gravel size D (c) Denudation increases with decreasing competent gravel fraction in the denuded material ω; (d) The profile of main stem denudation rate is mostly stretched in the horizontal as drainage area A increases; (e) Range of mean main-stem denudation rates obtained by varying each parameter, with the vertical tick indicating the Base Case values; (f) denudation profiles for the tested ranges of i_{flood}, D and ω. Shaded envelopes denote the full parameter ranges, and solid lines represent the Base Case.

The results given above are based on the generic REFL which includes empirical input for the evaluation of the hydrologic coefficient i_{flood} and the hillslope parameters L_h and S_h that are specific to the Britain II dataset mentioned above. We next apply the proposed denudation framework to DEMs of five catchments from this dataset. The five DEMS are shown in Figure 4a-4e, and the corresponding predicted patterns of denudation rate are shown in Figures 4f-4j. The values of i_{flood}, D, ω are arbitrarily chosen to be the same as the Base Case here; the denudation results with site-specific data are shown in supporting Figure S5 and Table S2.

Figure 4k shows the main-stem profiles, and Figure 4l the corresponding main-stem denudation rates. Maximum denudation rates are similar across the five basins because they occur at channel heads with the same minimum drainage area, whereas minimum rates vary among basin outlets and decrease with basin size (Figure 4l). For reference, Figure 4m compares the hypsometric curves of the five natural basins with the Base Case REFL. Their close agreement indicates that the Base Case REFL is representative of natural basins with similar characteristics.

Direct field evaluations of denudation rates are not available for any of these five catchments. In addition, several of the input parameters used to generate the main denudation profiles in Figure 4l are realistic but arbitrary. It is, however, possible to test whether the predicted values fall in the range of observed values for British lowland landscapes. Clayton (1997) quotes mean denudation rates for five regions in Britain (not the same as the five British catchments of Figures 4a to 4e) ranging from 0.009 mm/year to 0.132 mm/year (Table 1 therein; denudation by all processes). The predicted range for main stem denudation rates seen in Figure 4l is 0.015 mm/year (channel mouth) to 0.24 mm/year (channel head). The corresponding mean denudation rates predicted for these catchments range from 0.12 mm/year to 0.14 mm/year, thus falling within the range quoted by Clayton (1997).

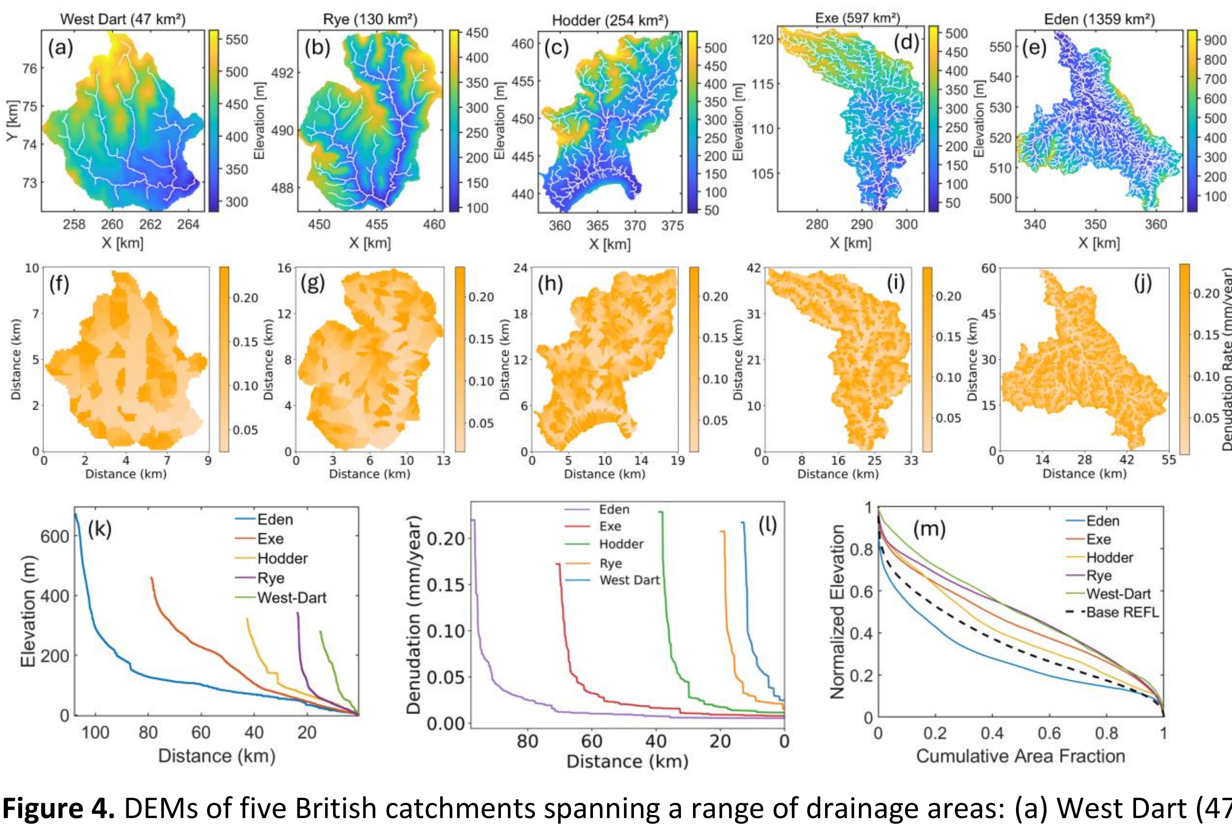

Figure 4. DEMs of five British catchments spanning a range of drainage areas: (a) West Dart (47 km²), (b) Rye (130 km²), (c) Hodder (254 km²), (d) Exe (597 km²), and (e) Eden (1359 km²). (f-j) Corresponding denudation rates computed using the proposed framework after resampling the original 10 m DEMs to 100 m resolution for model implementation. (k) Main stem profiles for five basins (l) Computed denudation rates along each of the main stem channel profiles (m) Hypsometric curves for each of the five catchments, along with that for the Base Case REFL.

4 Discussion

Denudation is a complex process involving bedrock weathering, regolith evolution, and sediment transport by hillslope processes such as creep, landsliding, tree throw, and bioturbation (Li et al., 2025; Rempe & Dietrich, 2014; Sklar, 2024). Although our framework does not explicitly model hillslope processes, it assumes that, under quasi-equilibrium conditions, long-term sediment production balances river sediment export. Denudation is therefore inferred from the gravel transport capacity of channels draining adjacent hillslopes. By linking channel hydraulics with sediment transport, it provides spatially distributed denudation estimates across entire catchments rather than basin-averaged values from a limited number of sampling sites.

The proposed framework provides denudation estimates using a minimal set of readily obtainable inputs: drainage area, hydraulic geometry, characteristic gravel size, and the gravel fraction of denuded material. The predicted downstream decline in denudation agrees qualitatively with cosmogenic ^{10}Be observations showing higher erosion rates in smaller upstream basins (Abbühl et al., 2010; Deng et al., 2020). This qualitative agreement suggests that hydraulic geometry-controlled sediment transport captures an important first-order control on denudation.

Sensitivity analyses indicate a clear separation between controls on denudation pattern and magnitude (see Figs. S1-S4). Drainage network organization establishes the persistent spatial template, producing systematically decreasing denudation downstream regardless of parameter values. In contrast, hydraulic and sediment parameters (i_{flood}, D, and ω) primarily scale denudation magnitude without altering this spatial structure. This suggests that drainage topology governs first-order spatial variability, whereas climate and sediment properties determine erosion intensity. This separation suggests that predictive models can leverage network structure to constrain spatial patterns of denudation even under uncertain hydrologic or sediment conditions. More broadly, it underscores the importance of explicitly representing drainage network organization when scaling erosion processes from local channel dynamics to catchment-scale landscape evolution.

The present analysis includes several simplifying assumptions that define its scope. The framework is intended for low-slope, tectonically subdued montane catchments in quasi-equilibrium that are drained by alluvial gravel-bed rivers. Bankfull discharge is assumed to scale linearly with drainage area following the Rational Method, providing a practical approximation, although more detailed hydrologic models or site-specific discharge and precipitation data could improve estimates where runoff generation or land cover vary substantially. The model further assumes constant characteristic gravel size, gravel fraction of denuded material, and flood intermittency factor throughout the catchment. Consequently, downstream fining, spatial variability in regolith composition, mixed bedrock–alluvial channels, and temporal variations in hydrologic forcing and varying lithology are not represented, and the predicted denudation rates reflect quasi-equilibrium conditions tied to present hydraulic regimes. While these assumptions are reasonable for the relatively small catchments considered here, extensions incorporating downstream fining (An et al., 2024), hydraulic geometry for mixed bedrock–alluvial channels (Wright et al., 2022), and bedrock incision and bedrock–alluvial morphodynamics (Zhang, Parker, et al., 2026), together with improved hydrologic inputs and variable sediment properties, would broaden the framework to a wider range of geomorphic settings, including tectonically active catchments.

5 Conclusion

We present a sediment-flux-based framework that links reach-scale gravel transport to spatially distributed denudation. Applied to reverse-engineered landscapes, the framework predicts systematic downstream decreases in denudation and quantifies the effects of drainage-network organization, catchment area, grain size, precipitation, and the gravel fraction of denuded material. Denudation increases with precipitation and characteristic grain size but decreases with increasing competent-gravel fraction. Application to five British catchments produces denudation rates consistent with regional field estimates, demonstrating that the framework can also be applied to specific catchments where suitable topographic and channel data are available. The framework provides a computationally efficient means of estimating spatial erosion patterns where direct measurements are limited. Although demonstrated for tectonically subdued montane catchments with alluvial gravel-bed streams, its conceptual structure could be extended to uplifting landscapes by incorporating mixed bedrock-alluvial hydraulic geometry, incision, bedrock-alluvial transitions, and downstream sediment fining.

Acknowledgments

A.S. acknowledges partial support from NSF EAR- 2342936 and D.B. to UCF Preeminent Postdoctoral Program (P3) fellowship.

Open Research

The software used to generate 2D networks is available at Borse (2026a), and that used to generate 3D landscapes is available at Borse (2026b). Sample data and algorithm to calculate denudation is available at Borse (2026c).

Conflict of Interest Disclosure

The authors declare there are no conflicts of interest for this manuscript.

References

Abbühl, L. M., Norton, K. P., Schlunegger, F., Kracht, O., Aldahan, A., & Possnert, G. (2010). El Niño forcing on 10Be-based surface denudation rates in the northwestern Peruvian

Andes? *Geomorphology*, *123*(3–4), 257–268. https://doi.org/10.1016/J.GEOMORPH.2010.07.017

An, C., Parker, G., Venditti, J. G., Lamb, M. P., Hassan, M. A., Miwa, H., & Fu, X. (2024). Autogenic Formation of Bimodal Grain Size Distributions in Rivers and Its Contribution to Gravel-Sand Transitions. *Geophysical Research Letters*, *51*(17), e2024GL109109. https://doi.org/10.1029/2024GL109109

Anderson, R. S., & Anderson, S. P. (2010). Geomorphology: The Mechanics and Chemistry of Landscapes. https://doi.org/10.1017/CBO9780511794827

Anderson, S. P., Dietrich, W. E., & Brimhall, G. H. (2002). Weathering profiles, mass-balance analysis, and rates of solute loss: Linkages between weathering and erosion in a small, steep catchment. *GSA Bulletin*, *114*(9), 1143–1158. https://doi.org/10.1130/0016-7606(2002)114<1143:WPMBAA>2.0.CO;2

Attal, M., Mudd, S. M., Hurst, M. D., Weinman, B., Yoo, K., & Naylor, M. (2015). Impact of change in erosion rate and landscape steepness on hillslope and fluvial sediments grain size in the Feather River basin (Sierra Nevada, California). *Earth Surf. Dynam*, *3*, 201–222. https://doi.org/10.5194/esurf-3-201-2015

Bierman, P. R., & Nichols, K. K. (2004). Rock to Sediment-Slope to Sea with 10Be-Rates of Landscape Change. *Annu. Rev. Earth Planet. Sci*, *32*, 215–255. https://doi.org/10.1146/annurev.earth.32.101802.120539

von Blanckenburg, F. (2005). The control mechanisms of erosion and weathering at basin scale from cosmogenic nuclides in river sediment. *Earth and Planetary Science Letters*, *237*(3–4), 462–479. https://doi.org/10.1016/J.EPSL.2005.06.030

Borse, D., & Biswal, B. (2023). A novel probabilistic model to explain drainage network evolution. *Advances in Water Resources*, *171*. https://doi.org/10.1016/j.advwatres.2022.104342

Borse, D. (2026a). ProCNE: Probabilistic Channel Network Evolution Model (Version v1.1). [Software]. *Zenodo*. https://doi.org/10.5281/zenodo.19935428

Borse, D. (2026b). dvborse/Create_3D_landscape_from_2D_drainage_network (Version v1.0). [Software]. *Zenodo*. https://doi.org/10.5281/zenodo.19950886

Borse, D. (2026c). Model for Reconstructing Spatial Denudation Patterns in Fluvial Landscapes (Version v1.0). Zenodo. https://doi.org/10.5281/zenodo.21500224

Brown, E. T., Stallard, R. F., Larsen, M. C., Raisbeck, G. M., & Yiou, F. (1995). Denudation rates determined from the accumulation of in situ-produced 10Be in the luquillo experimental forest, Puerto Rico. *Earth and Planetary Science Letters*, *129*(1–4), 193–202. https://doi.org/10.1016/0012-821X(94)00249-X

Clayton, K. M. (1997). The rate of denudation of some British lowland landscapes. *Earth Surface Processes and Landforms*, *22*(8), 721–731. https://doi.org/10.1002/(SICI)1096-9837(199708)22:8<721::AID-ESP741>3.0.CO;2-2

Davis, W. M. (1899). The Geographical Cycle. *The Geographical Journal*, *14*(5), 481–504. Retrieved from https://doi.org/10.2307/1774538

Deng, K., Yang, S., von Blanckenburg, F., & Wittmann, H. (2020). Denudation Rate Changes Along a Fast-Eroding Mountainous River With Slate Headwaters in Taiwan From ^{10}Be (Meteoric)/ ^{9}Be Ratios. *Journal of Geophysical Research: Earth Surface*, *125*(2), e2019JF005251. https://doi.org/10.1029/2019JF005251

Dietrich, W. E., Bellugi, D. G., Sklar, L. S., Stock, J. D., Heimsath, A. M., & Roering, J. J. (2013). Geomorphic Transport Laws for Predicting Landscape form and Dynamics. In *Geophysical Monograph Series* (Vol. 135, pp. 103–132). Blackwell Publishing Ltd. https://doi.org/10.1029/135GM09

Granger, D. E., Kirchner, J. W., & Finkel, R. (1996). Spatially Averaged Long-Term Erosion Rates Measured from in Situ-Produced Cosmogenic Nuclides in Alluvial Sediment. *The Journal of Geology*, *104*(3), 249–257. https://doi.org/10.1086/629823

Hey, R. D., & Thorne, C. R. (1986). Stable Channels with Mobile Gravel Beds. *Journal of Hydraulic Engineering*, *112*(8), 671–689. https://doi.org/10.1061/(ASCE)0733-9429(1986)112:8(671)

Howard, A. D. (1994). A detachment-limited model of drainage basin evolution. *Water Resources Research*, *30*(7), 2261–2285. https://doi.org/10.1029/94WR00757

Lal, D. (1991). Cosmic ray labeling of erosion surfaces: in situ nuclide production rates and erosion models. *Earth and Planetary Science Letters*, *104*(2–4), 424–439. https://doi.org/10.1016/0012-821X(91)90220-C

Leopold, L. B., & Maddock, T. (1953). *The hydraulic geometry of stream channels and some physiographic implications*. https://doi.org/10.3133/pp252

Li, T., Sklar, L. S., & Gasparini, N. M. (2025). Hillslope grain size variation across evolving landscapes linked to climate, tectonics and lithology. *Earth Surface Processes and Landforms*, *50*(8), e70111. https://doi.org/10.1002/esp.70111

Milliman, J. D., & Syvitski, J. P. M. (1992). Geomorphic/Tectonic Control of Sediment Discharge to the Ocean: The Importance of Small Mountainous Rivers. *The Journal of Geology*, *100*(5), 525–544. https://doi.org/10.1086/629606

Montgomery, D. R., & Brandon, M. T. (2002). Topographic controls on erosion rates in tectonically active mountain ranges. *Earth and Planetary Science Letters*, *201*(3–4), 481–489. https://doi.org/10.1016/S0012-821X(02)00725-2

Paola, C., Heller, P. L., & Angevine, C. L. (1992). The large-scale dynamics of grain-size variation in alluvial basins, 1: Theory. *Basin Research*, *4*(2), 73–90. https://doi.org/10.1111/J.1365-2117.1992.TB00145.X

Parker, G., Wilcock, P. R., Paola, C., Dietrich, W. E., & Pitlick, J. (2007). Physical basis for quasi-universal relations describing bankfull hydraulic geometry of single-thread gravel bed rivers. *Journal of Geophysical Research: Earth Surface*, *112*(4). https://doi.org/10.1029/2006JF000549

Parker, G., An, C., Lamb, M. P., Garcia, M. H., Dingle, E. H., & Venditti, J. G. (2024). Dimensionless argument: a narrow grain size range near 2mm plays a special role in river sediment transport and morphodynamics. *Earth Surface Dynamics*, *12*(1), 367–380. https://doi.org/10.5194/ESURF-12-367-2024

Portenga, E. W., & Bierman, P. R. (2011). Understanding earth's eroding surface with 10Be. *GSA Today*, *21*(8), 4–10. https://doi.org/10.1130/G111A.1

Reiners, P. W., & Brandon, M. T. (2007). Using Thermochronology to Understand Orogenic Erosion. https://doi.org/10.1146/ANNUREV.EA.34.080307.200001

Rempe, D. M., & Dietrich, W. E. (2014). A bottom-up control on fresh-bedrock topography under landscapes. *Proceedings of the National Academy of Sciences*, *111*(18), 6576–6581. https://doi.org/10.1073/pnas.1404763111

Sklar, L. S. (2024). Grain Size in Landscapes. *Annual Review of Earth and Planetary Sciences*, *52*(1), 663–692. https://doi.org/10.1146/annurev-earth-052623-075856

Summerfield, M. A. (2014). *Global Geomorphology*. *Global Geomorphology*. Routledge. https://doi.org/10.4324/9781315841182

Syvitski, J. P. M., & Milliman, J. D. (2007). Geology, Geography, and Humans Battle for Dominance over the Delivery of Fluvial Sediment to the Coastal Ocean. *The Journal of Geology*, *115*(1), 1–19. https://doi.org/10.1086/509246

Tejedor, A., Singh, A., Zaliapin, I., Densmore, A. L., & Foufoula-Georgiou, E. (2017). Scale-dependent erosional patterns in steady-state and transient-state landscapes. *Science Advances*, *3*(9). https://doi.org/10.1126/sciadv.1701683

Tucker, G. E., & Hancock, G. R. (2010). Modelling landscape evolution. *Earth Surface Processes and Landforms*, *35*(1), 28–50. https://doi.org/10.1002/esp.1952

Turowski, J. M., Rickenmann, D., & Dadson, S. J. (2010). The partitioning of the total sediment load of a river into suspended load and bedload: a review of empirical data. *Sedimentology*, *57*(4), 1126–1146. https://doi.org/10.1111/j.1365-3091.2009.01140.x

Whipple, K. X. (2004). Bedrock Rivers and the Geomorphology of Active Oregons. *Annual Review of Earth and Planetary Sciences*, *32*(1), 151–185. https://doi.org/10.1146/annurev.earth.32.101802.120356

Whipple, K. X., & Tucker, G. E. (1999). Dynamics of the stream-power river incision model: Implications for height limits of mountain ranges, landscape response timescales, and research needs. *Journal of Geophysical Research: Solid Earth*, *104*(B8), 17661–17674. https://doi.org/10.1029/1999jb900120

Whipple, K. X., & Tucker, G. E. (2002). Implications of sediment-flux-dependent river incision models for landscape evolution. *Journal of Geophysical Research: Solid Earth*, *107*(B2), ETG 3-1. https://doi.org/10.1029/2000JB000044

Wilkerson, G. V., & Parker, G. (2010). Physical Basis for Quasi-Universal Relationships Describing Bankfull Hydraulic Geometry of Sand-Bed Rivers. *Journal of Hydraulic Engineering*, *137*(7), 739–753. https://doi.org/10.1061/(ASCE)HY.1943-7900.0000352

Willett, S. D., & Brandon, M. T. (2002). On steady states in mountain belts. *Geology*, *30*(2), 175. https://doi.org/10.1130/0091-7613(2002)030<0175:OSSIMB>2.0.CO;2

Willgoose, G., Bras, R. L., & Rodriguez-Iturbe, I. (1991). A coupled channel network growth and hillslope evolution model: 1. Theory. *Water Resources Research*, *27*(7), 1671–1684. https://doi.org/10.1029/91WR00935

Wright, M., Venditti, J. G., Li, T., Hurson, M., Chartrand, S., Rennie, C., & Church, M. (2022). Covariation in width and depth in bedrock rivers. *Earth Surface Processes and Landforms*, *47*(6), 1570–1582. https://doi.org/10.1002/esp.5335

Zhang, L., Borse, D., Singh, A., Pizzuto, J. E., Fu, X., & Parker, G. (2026). Hydraulic geometry hypothesis allows reverse engineering of 3D quasi-equilibrium landscapes from 2D channel networks: Earth, Mars, Titan. *Proceedings of the National Academy of Sciences*, *123*(21). https://doi.org/10.1073/pnas.2513733123

Zhang, L., Parker, G., Nittrouer, J., Fu, X., Zhang, S., & Wang, G. (2026). Linked Canyons and Fans Communicate Through a Migrating Bedrock-Alluvial Transition. *Journal of Geophysical Research: Earth Surface*, *131*(6), e2025JF008718. https://doi.org/10.1029/2025JF008718

Supporting Information for

Reconstructing Spatial Denudation Patterns in a Reverse-Engineered Fluvial Catchment

Dnyanesh Borse[1], Arvind Singh[1], and Gary Parker[2,3]

[1]Department of Civil, Environmental, and Construction Engineering, University of Central Florida, Orlando, FL, USA.

[2]Dept. of Earth Science and Environmental Change, University of Illinois Urbana-Champaign, Urbana, IL 61801.

[3]Dept. of Civil and Environmental Engineering, University of Illinois Urbana-Champaign, Urbana, IL 61801.

Contents of this file

Text S1 to S2
Figures S1 to S5
Tables S1 to S2

Introduction

SI text includes detailed methods to obtain the reverse engineered fluvial landscape (REFL) using the methodology of Zhang et al., (2026a). It also contains additional figures corresponding to sensitivity analyses and modelled denudation in British basins using observed bankful discharge and grain size.

Text S1 Simulating Reverse Engineered Generic Landscape

To demonstrate the proposed denudation framework, we employ the Reverse Engineered Fluvial Landscape (REFL) methodology developed by Zhang et al. (2026a) that constructs 3D landscape and channel properties using 2D drainage network based on physically based relationships. The REFLs generated by them represent a class of low-relief montane catchments with subdued tectonics drained by alluvial gravel-bed rivers. The REFL framework consists of three components: (a) a two-parameter probabilistic model for generating scale-free two-dimensional drainage networks (Borse and Biswal, 2023), (b) physically based dimensionally homogeneous hydraulic geometry relations for alluvial gravel-bed rivers (Parker et al., 2007) and (c) a simplified hillslope representation capturing processes toward the headwaters, including below capacity transport and landsliding, which is characterized by an effective hillslope length L_h and hillslope slope S_h calibrated using the Britain II dataset (Hey & Thorne, 1986; Zhang et al., 2026a).

The probabilistic model of Borse and Biswal (2023) generates scale-free drainage networks that reproduce the statistical properties of natural river systems (See Fig.1a). These dimension-free networks are subsequently scaled to physical dimensions with length scales in km using the multiplicative scaling parameter λ. These scaled networks are combined with hydraulic geometry relations to compute channel slope S, bankfull width B_{bf}, bankfull depth H_{bf}, and bankfull gravel transport rate $Q_{b,bf}$ as functions of bankfull discharge Q_{bf} and characteristic surface grain size D (Parker et al., 2007).

Once these parameters are specified, the reverse-engineering procedure generates a three-dimensional landscape with elevations (Figs. 1b and 1c), channel widths, depths, discharges, and gravel transport rates defined throughout the drainage network. Two simplifications are adopted here: (1) all channels within a catchment are characterized by a single representative surface grain size D, and (2) the effects of mixed bedrock-alluvial reaches in the headwaters are incorporated into an effective hillslope model with a deliberately enlarged hillslope length (Zhang et al., 2026a).

Text S2 Estimation of Bankfull Discharge $\left(Q_{bf}\right)$

Bankfull discharge, Q_{bf}, is estimated from the upstream drainage area, A, using an empirical area–discharge relationship. Following the Rational Method commonly used in hydrology, discharge is assumed to increase linearly with drainage area:

$$Q_{\mathrm{bf}} = aA,$$

where A is expressed in km^2, Q_{bf} in $\mathrm{m}^3\ \mathrm{s}^{-1}$, and a is a regional discharge-scaling coefficient with units of $\mathrm{m}^3\ \mathrm{s}^{-1}\ \mathrm{km}^{-2}$. This formulation assumes that the hydrologic conditions controlling bankfull discharge are spatially uniform within a catchment. Consequently, differences in Q_{bf} among channel locations arise from differences in their contributing drainage areas. To explicitly represent the hydroclimatic controls included within a, the relationship is expanded as

$$Q_{\mathrm{bf}} = a_{\mathrm{flood}}\, i_{\mathrm{flood}}\, I_{\mathrm{flood}}\, A, \qquad a = a_{\mathrm{flood}}\, i_{\mathrm{flood}}\, I_{\mathrm{flood}},$$

where i_{flood} is the effective precipitation intensity associated with near-bankfull events, I_{flood} is flood intermittency, defined as the fraction of time that the river experiences near-bankfull flow, and a_{flood} is a dimensionless coefficient accounting for the fraction of precipitation contributing to channel discharge. Consistent units and the required area conversion are used when evaluating Equation (S1b).

For the reference condition, we use $a = 0.518\ \mathrm{m}^3\ \mathrm{s}^{-1}\ \mathrm{km}^{-2}$, empirically derived by Zhang et al. (2026a) from the Britain II dataset of gravel-bed rivers (Hey & Thorne, 1986) and correspondingly i_{flood} and I_{flood} were assumed to be 2.59 mm/hr and 0.01 respectively. Thus, the bankfull discharge assigned to every channel location is calculated from its upstream contributing area as

$$Q_{\mathrm{bf}} = 0.518A.$$

This area–discharge relationship provides the hydrologic input to the hydraulic geometry relations used to calculate channel slope, bankfull width and depth, and bankfull gravel-transport rate throughout the drainage network.

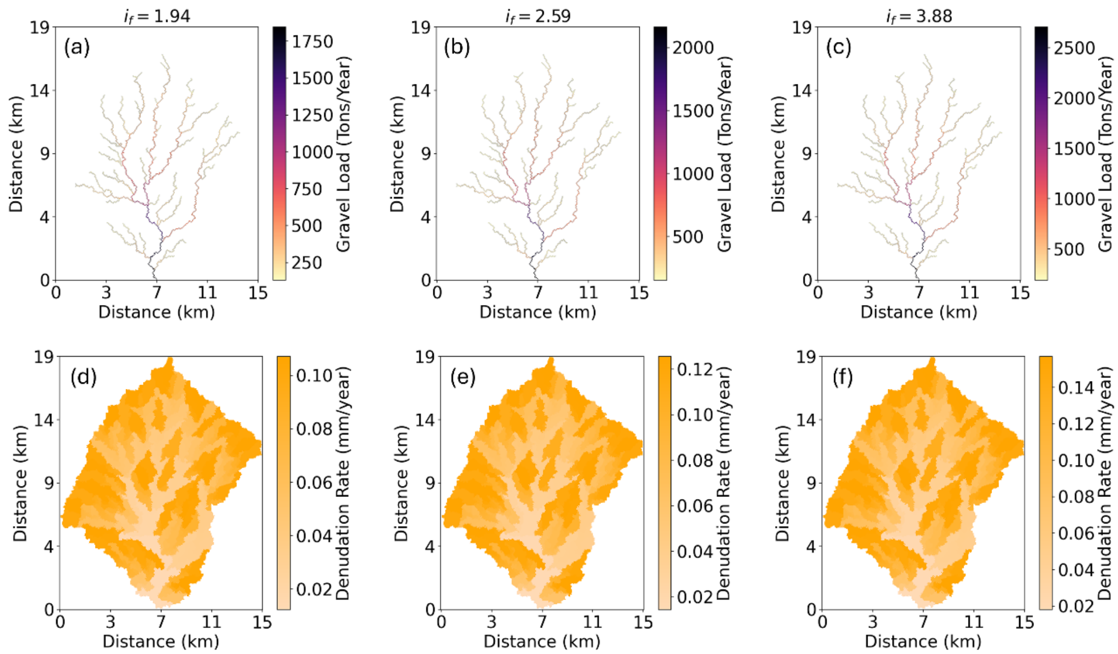

Figure S1. Sensitivity of gravel load and denudation rate to effective precipitation intensity (i_f). Spatial distributions of mean annual gravel load (a–c) and denudation rate (d–f) for $i_f = 1.94$, 2.59, and 3.88 mm/hr, respectively. Increasing i_f increases bankfull discharge and gravel-transport capacity, resulting in higher denudation rates while preserving the overall spatial pattern. All other model parameters are held constant. Note that the color-bar ranges vary among columns to show the spatial variation within each simulation.

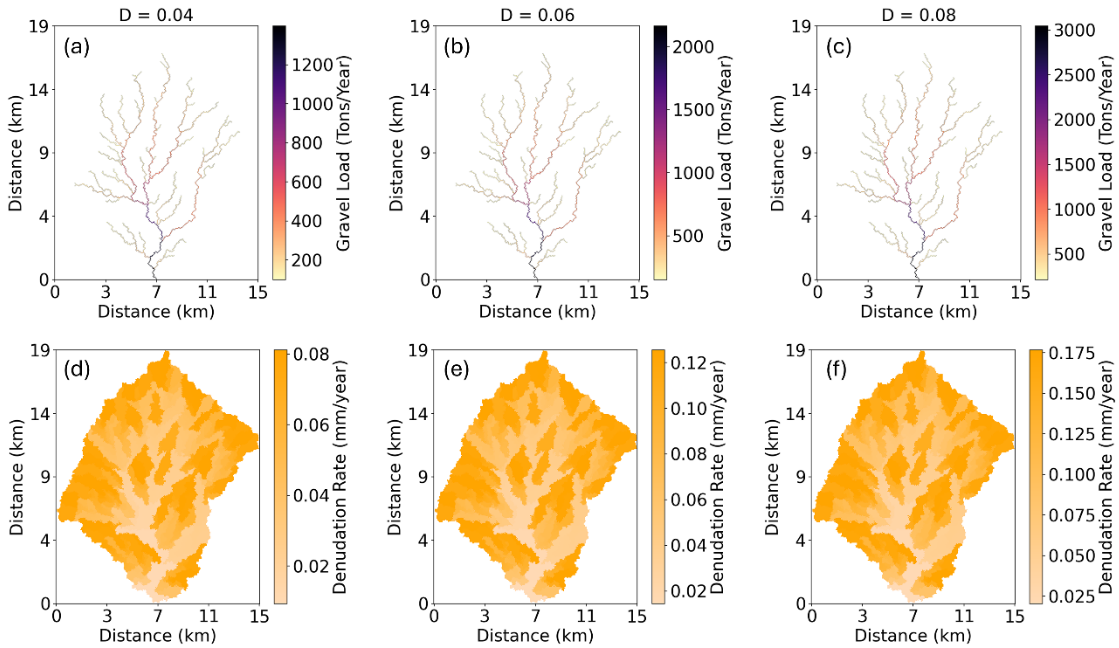

Figure S2. Sensitivity of gravel load and denudation rate to characteristic surface grain size (D). Spatial distributions of mean annual gravel load (a–c) and denudation rate (d–f) for $D = 0.04$, 0.06, and 0.08 m, respectively. Increasing D increases the predicted gravel load and corresponding denudation rates.

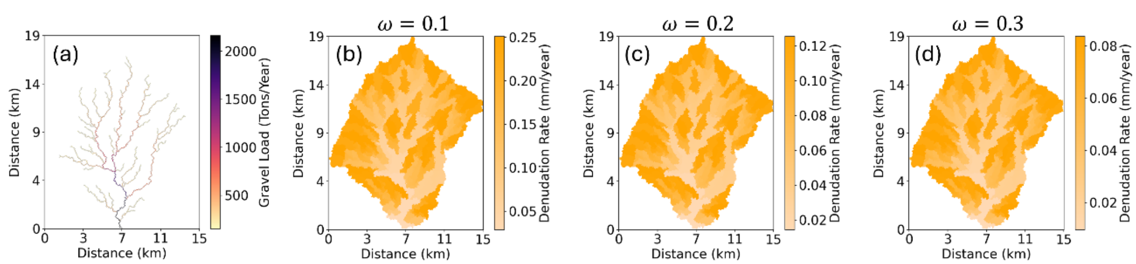

Figure S3. Sensitivity of denudation rate to the competent-gravel fraction ($\boldsymbol{\omega}$). Panel (a) shows the mean annual gravel load, while panels (b–d) show the corresponding denudation rates assuming that competent gravel constitutes ω =0.1, 0.2, and 0.3 of the total denuded sediment, respectively. Increasing the competent-gravel fraction reduces the denudation rate required to supply the same channel gravel load.

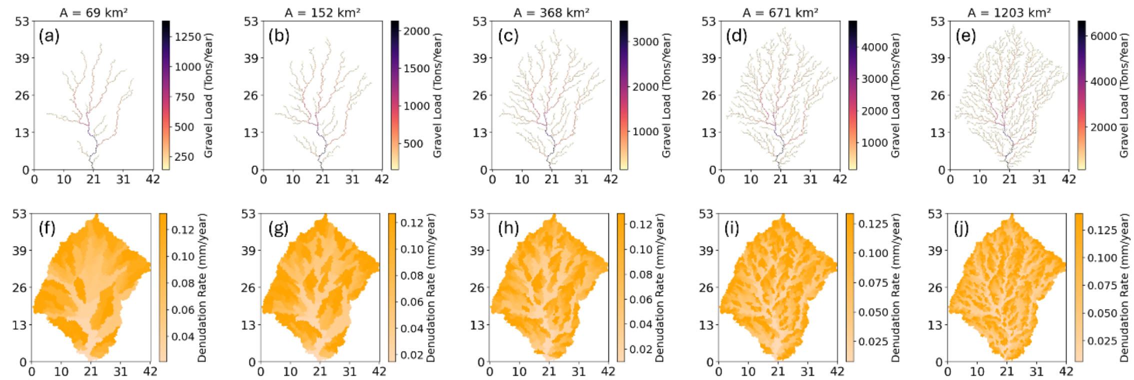

Figure S4. Sensitivity of gravel load and denudation rate to catchment area (A). Spatial distributions of mean annual gravel load (a–e) and denudation rate (f–j) for catchment areas of 69, 152, 368, 671, and 1,203 km^2, respectively. Gravel load increases with catchment area because of the corresponding increase in contributing area and bankfull discharge. Maximum denudation rates remain similar across the five catchments because they occur near channel heads with the same minimum drainage area, whereas minimum rates occur near the catchment outlet and decrease with increasing catchment area.

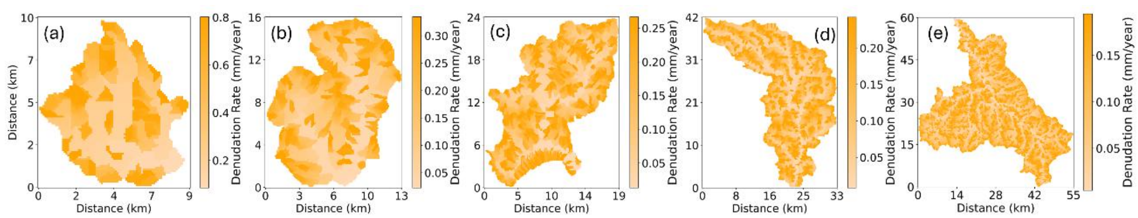

Figure S5. Application of the denudation framework to five British catchments using observed bankfull discharge and characteristic gravel size as given in table S2.

Input Parameter	Value	Min Det (mm/year)	Max Det (mm/year)	Mean Det (mm/year)
i_{flood} (mm/hr)	1.94	0.012	0.107	0.039
	2.59	0.014	0.126	0.046
	3.88	0.018	0.157	0.057
D (m)	0.04	0.009	0.081	0.030
	0.06	0.014	0.126	0.046
	0.08	0.020	0.177	0.065
ω	0.1	0.029	0.251	0.092
	0.2	0.014	0.126	0.046
	0.3	0.010	0.084	0.031
A (km2)	69	0.021	0.123	0.059
	152	0.015	0.127	0.046
	368	0.010	0.123	0.035
	671	0.007	0.121	0.028
	1203	0.006	0.132	0.023

Table S1. Summary of the sensitivity analysis showing the minimum, maximum, and mean of modeled denudation rates along the main stem obtained by varying each input parameter (i_{flood}, D, ω and A) over the tested ranges.

River	Drainage Area (Km2)	Qbf Observed (m3/s)	Qbf Modelled (m3/s)	D50 Observed (m)	Case 1 Det (mm/year)			Case 2 Det (mm/year)		
					Det Min	Det max	Det mean	Det Min	Det max	Det mean
West Dart	47	70.0	24.4	0.1758	0.025	0.217	0.070	0.084	0.740	0.239
Rye	130	100.0	67.5	0.0808	0.016	0.207	0.051	0.022	0.295	0.072
Hodder	254	348.0	131.8	0.066	0.011	0.229	0.035	0.013	0.259	0.040
Exe	597	154.0	309.4	0.0606	0.008	0.172	0.024	0.008	0.177	0.025
Eden	1359	424.0	703.8	0.0499	0.005	0.220	0.019	0.004	0.182	0.015

Table S2. Calculated denudation rates along the main stem for 5 sample British basins based on modelled Q_{bf} and constant D (case 1) and observed Q_{bf} and observed D (case 2). Case 1 corresponds to the characteristic grain size D = 0.059 m of the Base Case in the main text, whereas in Case 2 D is set to the observed value of surface D50. The large difference between the denudation values of Case 1 and Case 2 for the West Dart are mediated by the large difference in the assumed value of D.